Research Article

Sen Lin and Julian R. Jones*

The effect of serum proteins on apatite growth for 45S5 Bioglass and common sol-gel derived glass in SBF

https://doi.org/10.1515/bglass-2018-0002
Received Nov 08, 2017; revised Dec 05, 2017; accepted Dec 10, 2017

Abstract: The inhibitive effects of serum proteins on apatite growth was compared between melt-derived 45S5 Bioglass® and sol-gel derived bioactive glass of the 70S30C (70 mol% SiO_2, 30 mol% CaO). By using techniques of XRD, TEM and Raman spectroscopy, the transformation of amorphous calcium phosphate to crystalline apatite, and the resulting size and aspect ratio of the crystals, in simulated body fluid (SBF), was seen to decrease in the presence of serum. XRD showed more rapid HA formation on Bioglass particles, compared to that forming on 70S30C particles, however TEM showed similar size and frequency of the needle-like crystals. Phosphate reduction in SBF was similar for Bioglass and 70S30C. Calcium carbonate formation was more likely on the phosphate-free sol-gel glass than on Bioglass.

1 Introduction

Bioactive glasses have the ability of being able to bond to bone [1] without triggering formation of fibrous tissue through hydroxycarbonate apatite (HCA) formation on the glass surface, on contact with body fluid, which bonds to host bone via collagen interactions [2]. Bioactive glass dissolution products also stimulate bone regeneration at genetic level [2, 3]. Bioactive glass products have been developed into several medical device products and have been used in more than 1.5 million patients for orthopaedic indications [4]. Bioactive glasses are now being applied to soft tissue applications [5] and being developed into flexible hybrid materials [6].

Kokubo *et al.* [7] proposed simulated body fluid (SBF) to simulate ionic concentration of blood plasma [8] and it often used to compare HCA formation rates between bioactive glasses and other bioactive ceramics [9]. However, serum proteins have an important role to play in the dissolution rate of glasses and HCA formation rates. Apatite growth on 45S5 Bioglass® has been reported to be significantly inhibited with 10% serum incorporated in SBF [10]. Bioactive glasses can also be made via the sol-gel route [11–13], which also allows production of bioactive glass foam scaffolds [14, 15]. This study compares the inhibitive effects of proteins against apatite growth for two common bioactive glasses, made by the different routes of the melt-quench route and sol-gel process, and explores the mechanism of the HCA formation.

2 Experimental

Sol-gel glass of the 70S30C (70 mol% SiO_2, 30 mol% CaO) composition, also termed TheraGlass® (TG), and melt-quenched Bioglass® (BG, melt-derived 46.1 mol% SiO_2, 26.9 mol% CaO, 24.4 mol% Na_2O and 2.5 mol% P_2O_5), were provided by NovaThera Ltd. (Babraham, UK). Theraglass was produced by NovaThera using conventional processes of hydrolysis of tetraethylorthosilicate (TEOS) in water (molar ratio of water to TEOS, R ratio, of 12) [16] with nitric acid as the catalyst and calcium nitrate tertrahydrate as the calcium precursor and the glass was thermally stabilised at 700°C. All the glass samples were ground by a ball mill and passed through 38 μm sieves. Two media were used to study dissolution rate and apatite formation: pure SBF (pSBF) and SBF complemented with 10% foetal bovine serum FBS (sSBF). SBF was prepared following the previous method initially proposed by Kokubo [17]. FBS was purchased from Invitrogen™ (UK).

According to the recommended protocol by Maçon *et al.* [9], 75 mg of glass powders (BG and TG) were immersed in 50 ml of pSBF or sSBF at 37°C in an orbital incubator under agitation of 120 rpm. The samples were filtered after

***Corresponding Author: Julian R. Jones:** Department of Materials, Imperial College London, London, SW7 2BP, United Kingdom; Email: julian.r.jones@imperial.ac.uk
Sen Lin: Department of Materials, Imperial College London, London, SW7 2BP, United Kingdom

Open Access. © 2018 S. Lin and J. R. Jones, published by De Gruyter Open. BY-NC-ND This work is licensed under the Creative Commons Attribution-NonCommercial-NoDerivatives 4.0 License

Brought to you by | Imperial College London
Authenticated
Download Date | 4/4/19 12:57 PM

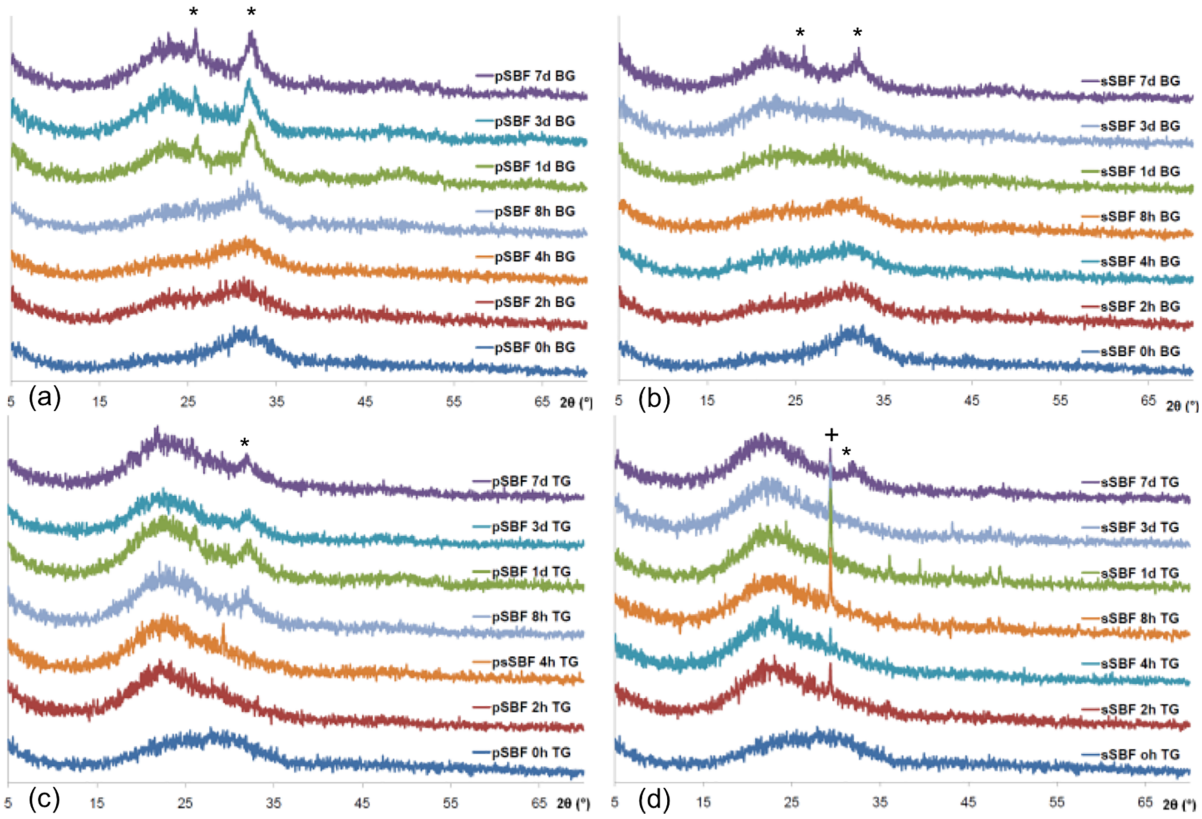


Figure 1: XRD patterns of (a,b) BG and TG (c,d) glass particles before and after immersion in pSBF (a,c) and sSBF (b,d), at different time points. * peaks at 26 and 32° 2θ corresponding to HA; + peaks correspond to calcite 29° 2θ.

a series times (2 h, 4 h, 8 h, 1 d, 3 d, and 7 d). Both the glass powders and filtered liquid were reserved for further analysis.

Transmission Electron Microscope (TEM, JEOL JEM-2010) was used to observe the surface layer formation on the glass particles. The samples for TEM were prepared by manually grinding into fine powders and mixing with acetone to prepare a powder suspension, into which a TEM sample support film was dipped and the film was dried in air. Energy Dispersive X-ray spectroscopy (EDX, within JEOL JEM-2000) chemical analysis, which was conducted within TEM was employed. X-Ray Diffraction (XRD, Philips PW1700, automated powder diffractometer) was used to analyse the crystal structure of the apatite formed on the surface of the glass particles. Cu K alpha radiation at 40 kV/40mA with a secondary graphite crystal monochromater was used. Regarding the parameters of the XRD scanning, the angular range, step size and counting time were from 5° to 70°, 0.04°, and 1 s, respectively. Raman microscope (inVia, Renishaw) was used to analyse and compare the substances formed on the glass surface. High power near infrared diode spot laser (100 mW at 785 nm air cooled, spot size approximately 1-3 µm) was used to conduct Raman scanning. Inductively Coupled Plasma (ICP, Thermo Scientific, iCAP 6300) was used to quantify the ion exchange between the glass particles and the medium of the bioactivity tests. All the ICP samples were diluted with 2 M HNO_3 and filtered with 0.2 µm filter.

2.1 Results and discussion

XRD was conducted to characterise any crystal structures that formed on the glass particles post immersion in pSBF and sSBF (Figure 1).

The mechanism of HCA growth on BG in SBF has been extensively studied [18]. Na^+ and Ca^{2+} from BG undergo cation exchange with H^+ from the media, leaving a silica rich gel-like layer at the glass surface and over-saturation of Ca in the media. The medium pH increased due to the cation exchange. Amorphous Ca/P compounds precipitate on the silica gel layer and crystallise into the needle-like HCA.

Here, peaks at approximately 26° and 32° 2θ were found in the XRD patterns of the filtered BG particles in

Brought to you by | Imperial College London
Authenticated
Download Date | 4/4/19 12:57 PM

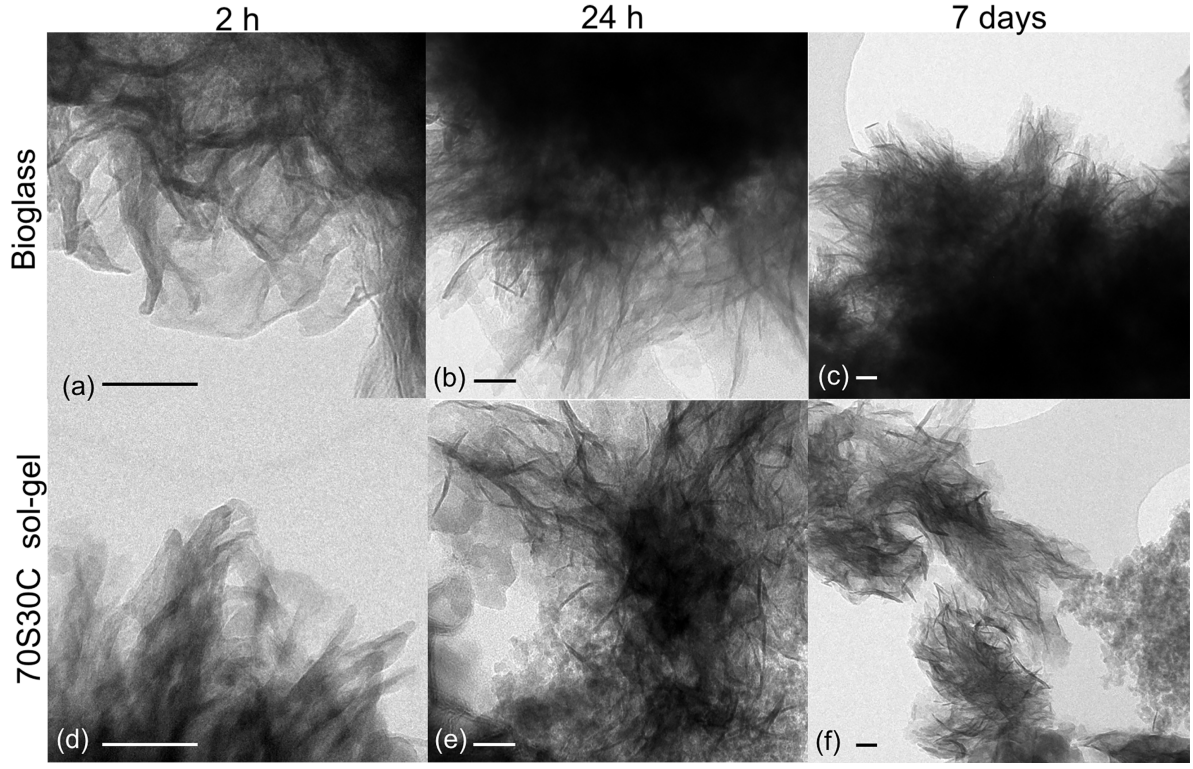


Figure 2: TEM images of BG (a, b, c) and TG (d, e, f) following immersion in pSBF for (a,d) 2 h; (b, e) 1 day; and (c, f) 7 days. Scale bars are 50 nm.

pSBF after 1 day of immersion and these peaks match the XRD pattern of hydroxylapatite (HA) [19]. Comparing the XRD patterns of BG (Figure 1a) and TG (Figure 1b) following immersion in pSBF, HA peaks did not appear for the TG glass until 7 day, compared to 1 day for BG, and the intensity and sharpness were less than for BG.

Slower HCA formation on TG could be due to the larger concentration of silica (network formers) in TG than BG, which resulted in a higher network connectivity (mean number of bridging Si-O-Si bonds per silicon atom) of TG (2.62 [16]) than BG (1.90 [20, 21]). The lower network connectivity of BG could enhance cation exchange increased the medium pH, which in turn improved Ca/P compound deposition. However, TG had a specific a surface area of 140 m^2 g^{-1} [22], compared to 0.24 m^2 g^{-1} [23] for BG, due to TG having a nanoporosity, with a modal pore diameter of 17.6 nm [22]. TEM showed that the HCA crystals were similar on TG compared with BG (Figure 2) and were of similar frequency, indicating that HCA formation rate was actually similar between the two types of glass. The higher surface area of TG is due to its nanoporosity and previous work showed protein such as fibrinogen can quickly penetrate the nanopores [22], so rapid adsorption of the serum proteins may have partially blocked the pores, reducing the benefit of the enhanced surface area, in terms of HCA formation.

Comparing XRD patterns of BG immersed in pSBF (Figure 1a) to BG in sSBF (Figure 1c), the inhibitive effects of serum against the apatite growth was confirmed since the HA peaks in the XRD patterns of BG immersed in sSBF had smaller intensities than those of BG immersed in pSBF. The HA peaks did not appear until 7 days of immersion in sSBF (Figure 1c) and the broader peak indicates the less and smaller dimension of the apatite crystals grown in sSBF compared to those formed in pSBF. The effects of serum on HA precipitation, which can be divided into effects on nucleation and crystal growth, are controversial. The effect on the nucleation, proteins were thought to cover the sites on the glass for apatite nucleation (Si-OH groups), inhibiting HCA nucleation [10]. However, it has also been proposed that proteins are polyelectrolytes, which provide more nucleation sites for apatite via calcium chelation. For the effects on the crystal growth, protein adsorption was considered a barrier for calcium and phosphate diffusion, which inhibited apatite crystal growth [10].

Here, serum exerted significant inhibitive effects on apatite growth on BG (Figure 1b). On TG, crystalline calcium carbonate was found in all the TG immersed in sSBF

Brought to you by | Imperial College London
Authenticated
Download Date | 4/4/19 12:57 PM

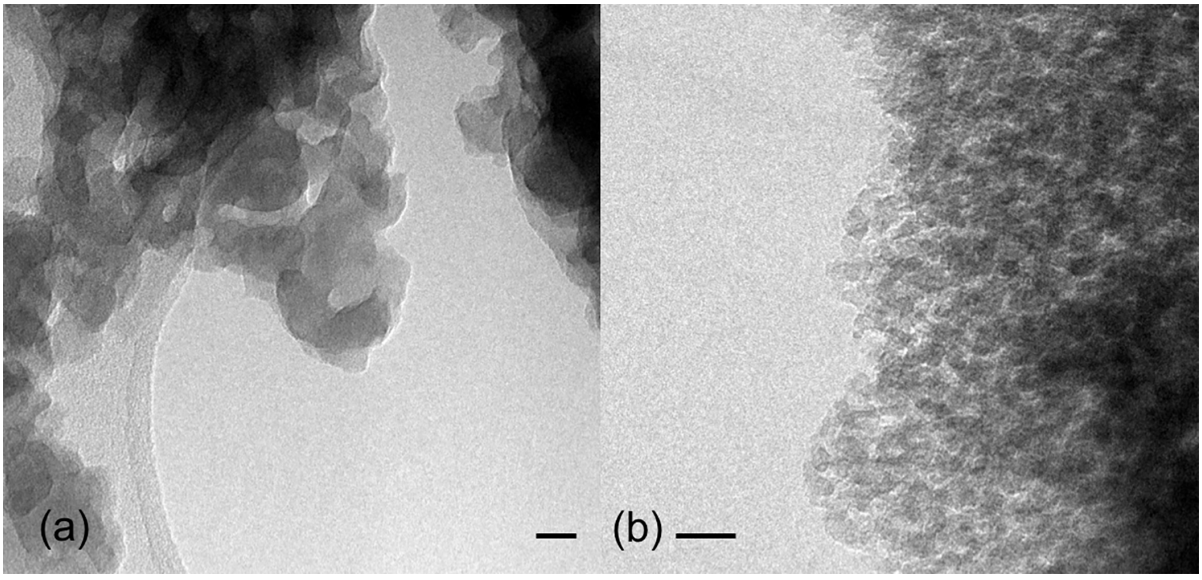


Figure 3: TEM images of TG particles (a) before immersion in pSBF; (b) after 2 h immersion in pSBF. Scale bar 20 nm.

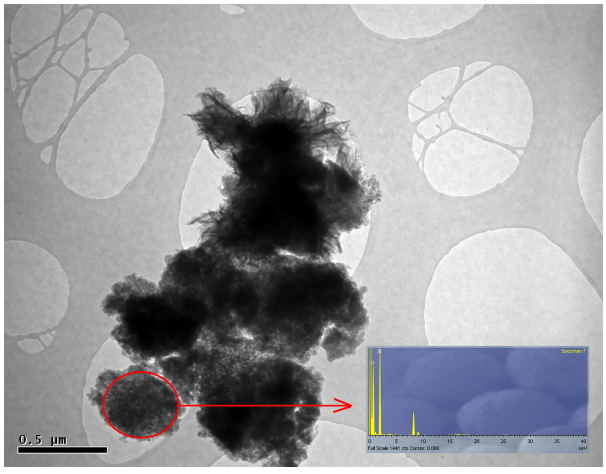


Figure 4: EDX analysis within TEM on TG after immersion in pSBF for 1 day. Peaks at 8-9 keV for Cu (TEM grid) not indexed.

(Figure 1d). This is previously observed when the sol-gel 58S (60 mol% SiO_2, 36 mol% CaO and 4 mol% P_2O_5) composition was immersed in culture media [24] and in SBF when the glass was in high concentration [25] and was thought to be due to the phosphate in the SBF being used up during calcium phosphate nucleation, leaving excess calcium that then reacts with carbonate in the media. This could explain large resorption pits formed by osteoclast cells on the surface of 70S30C foam scaffolds *in vitro* (osteoclasts would be expected to resorb calcium carbonate more rapidly than glass) [26]. Calcium carbonate formation was thought to not occur on BG due to the release of phosphate from the glasses (TG is phosphate-free). However the amount of phosphate present in the glass is very small compared to that available in SBF. It could be that the more rapid release of calcium from TG compared to BG, due to the higher surface area, caused local saturation of calcium in the SBF. Serum seems to promote calcium carbonate formation, which could be due to the proteins that are adsorbed onto TG surface chelate the calcium and hold it near the glass surface, enhancing calcium carbonate deposition.

TEM was used to confirm the existence of apatite crystals and observe the crystal morphology. TEM images of the BG particles following immersion show needle-like apatite crystals, approximately 5 nm in diameter and 30-100 nm in length, had grown on the surface of BG after 2 h immersion in pSBF. The morphology is similar with what previous researchers found [27].

The TG particles were covered in crystals of similar structure and dimension (Figure 2d-e), even after 2 h, even though HA peaks were not present in XRD patterns until 7 d. TEM images of TG particles (Figure 3) also show the nanoparticles (approximately 5 nm in diameter), of which the sol-gel derived TG consists. Following immersion in pSBF, the nanoparticle size of TG (termed tertiary particles in our previous study [16]) reduced from 10-30 nm to approximately 5 nm (Figure 1b).

This was confirmed by conducting EDX chemical analysis, within the TEM, on the nanostructure of TG after the particles immersed were in pSBF for 1 day (Figure 4).

The EDX result shows that the nanoparticles within the TG after immersion in pSBF for 1 day were composed of silica (the peaks at 8-9 keV represent copper, of which the TEM sample holder is composed). This verified that cal-

Brought to you by | Imperial College London
Authenticated
Download Date | 4/4/19 12:57 PM

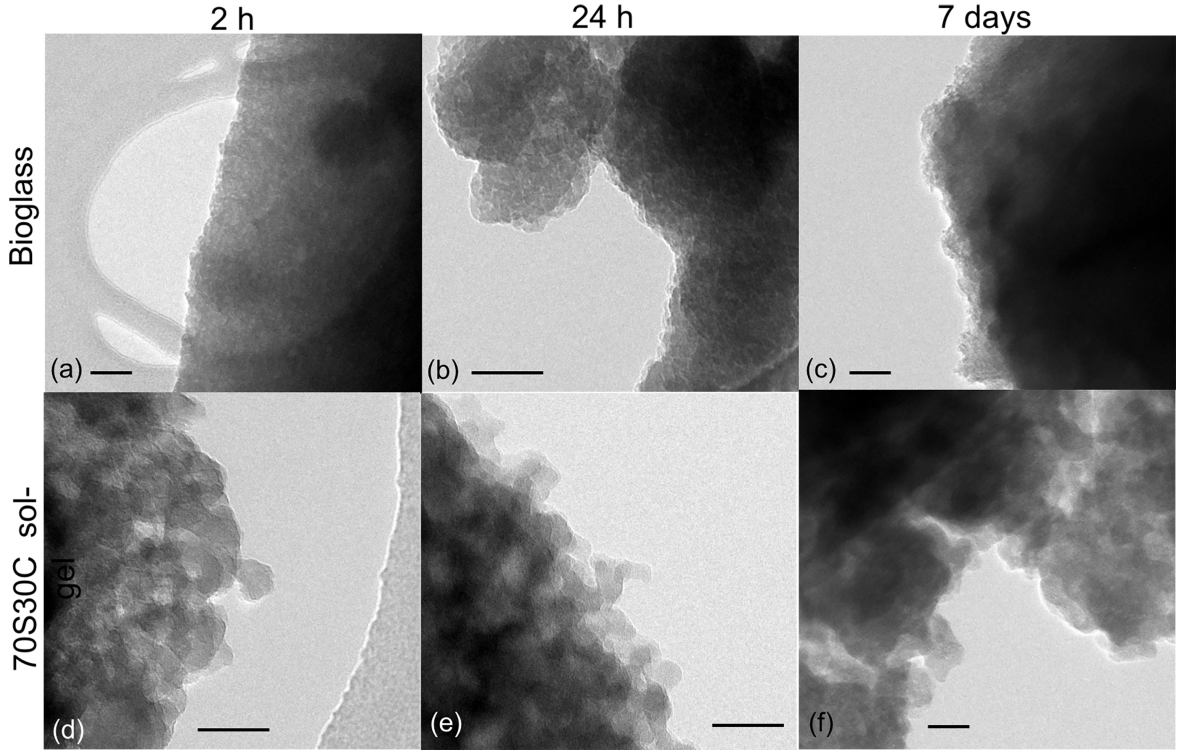


Figure 5: TEM images of BG (a, b, c) and TG (d, e, f) following immersion in sSBF for (a, d) 2 h; (b, e) 1 day (scale bar is 50 nm); and (c, f) 7 day. Scale bars are 50 nm.

cium in TG was depleted after immersion in pSBF, leaving a network of silica. This supports *in vivo* results on porous scaffolds of the same sol-gel derived bioactive glass (70 mol% SiO_2 and 30 mol% CaO), that calcium release is too rapid from that composition [28]. The *in vivo* results showed that, while the scaffolds were not toxic, the calcium dissolution inside the pore structure caused a pH rise that promoted bone growth around the scaffold, rather than through it. The nanoporosity enhances the calcium release rate compared to BG [14].

TEM images of BG particles following immersion in sSBF (Figure 5) showed that the needle-like apatite growth was inhibited. According to XRD, HA was not found until BG was immersed in the sSBF for 7 day, compared to 1 day in pSBF. TEM images showed that the apatite crystals were much smaller (approximately 5 nm in diameter and 10-20 nm in length) and less needle-like. Nanotexture was found on the surface of BG, which is due to the deposited bio-mineral layers.

The TEM images of the TG particles immersed in sSBF showed no HCA crystals within the 7 days of immersion. Interestingly, the tertiary nanoparticles that comprised TG were maintained in TG throughout the 7 days of immersion in sSBF, whereas they reduced in size during the same period in pSBF, indicating slower dissolution in sSBF. Calcite crystals were expected, but not observed in the regions imaged.

ICP was used to quantify the concentration of calcium, phosphate, and silicon in the media (Figure 6). In terms of the comparison between BG and TG, the calcium release rate of TG was much higher than BG, especially within the first 2 h of immersion, due to the nanoporosity, high surface area and slightly higher calcium content of TG. The silicon release rates of BG and TG were similar because the saturation of silicon was reached for both BG and TG 8 h after immersion. Serum proteins did not have a noticeable effect on the release of calcium and silicon. For phosphate, both BG and TG consumed phosphorous in pSBF within 2 h. This indicated that calcium phosphate precipitation rate was similar for both glasses (likely to be amorphous calcium phosphate formation initially). However, the calcium release was much higher for TG, triggering the co-precipitation of calcium carbonate (calcite). When the glasses were immersed in SBF, the phosphate of the sSBF was not consumed for either glass, even after 7 days. The low reduction rate of phosphate in sSBF from 8 h to 7 days indicates the slow deposition of apatite during this period with the inhibitive effects of serum.

Figure 7 shows the Raman spectra of BG and TG immersed in pSBF and sSBF. Raman spectroscopy is a power-

Brought to you by | Imperial College London
Authenticated
Download Date | 4/4/19 12:57 PM

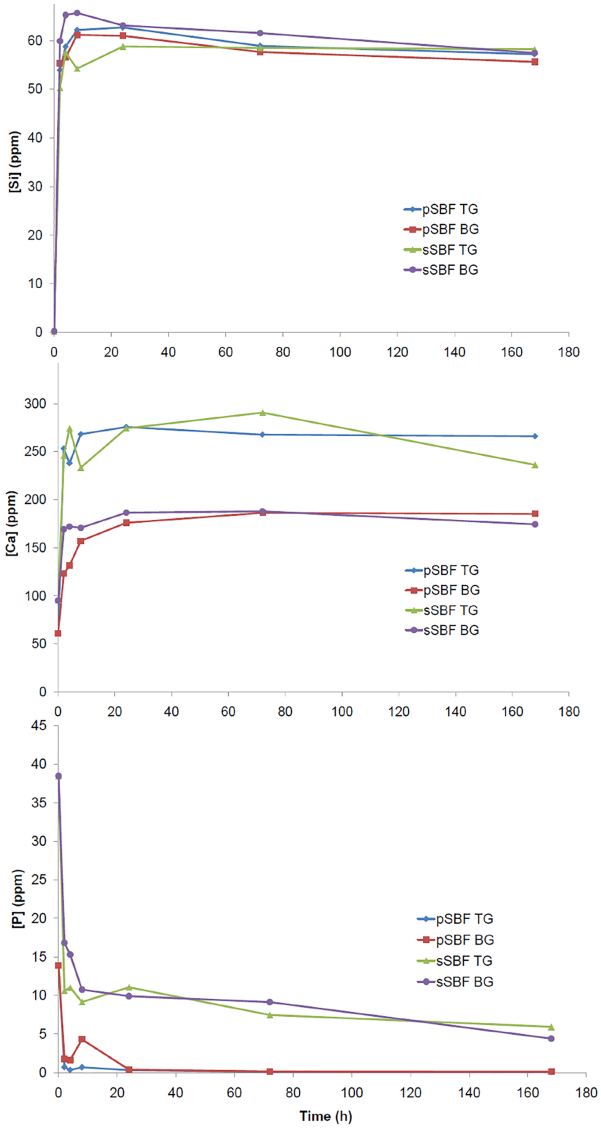


Figure 6: The concentration of silicon, calcium and phosphourous in the media as a function of immersion time of TG and BG.

ful tool to distinguish crystalline apatite from amorphous calcium phosphate (ACP). It is also very useful to characterise proteins. Orthophosphate peaks (indicative of HA) growth in the samples can be characterised from the P-O peaks at 1075, 960, 590, and 435 cm^{-1} whereas ACP is represented by the relatively broader P-O peaks at 1080, 950, and 630 cm^{-1} [29]. The existence of adsorbed proteins can be confirmed by the peaks at approximately 1660 (Amide I) and 1001 (C-C aromatic ring) cm^{-1} [30].

As the Raman spectra in Figure 7a shown, BG before immersion contains amorphous phosphate, which is indicated by the peaks at 950 and 630 cm^{-1}. The apatite growth occurred on BG after 2 h immersion in pSBF, which is indicated by the right-shift of peak at 630 to 590 cm^{-1} and the left-shift of the peak at 950 to 960 cm^{-1}. The shifts indicate that the apatite was likely to be directly derived from the apatite nucleation and crystal growth. This also indicates a better sensitivity of Raman spectroscopy than that of XRD in terms of nano-scale apatite crystals (XRD did not detect apatite crystal growth on BG in pSBF until 1 day of immersion).

By comparing Figure 7a and 7b, the apatite crystal growth in TG was slower than that in BG, since the P-O peaks did not appear until 1 day immersion in pSBF. Peaks related to ACP did not appear for TG throughout the process, so it is likely that any ACP deposited on TG in pSBF must have rapidly crystallised to HCA. The peak at 493 cm^{-1} only existed in the spectra of TG immersed in pSBF and this peak was reported related to the HO-Si-(O-)$_3$ tetrahedral vibration mode [31]. HO-Si-(O-)$_3$ is Q^3 silicon species (silicon atom connecting 1 non-bridging oxygen and 3 bridging oxygen), which contributes 23% of the whole silicon species according to NMR results in a previous study [16]. Calcium dissolved after immersed in pSBF, which transferred Ca-O-Si-(O-)$_3$ into HO-Si-(O-)$_3$ and contributed to the peak at 493 cm^{-1}. On the other hand, the network connectivity of BG is 1.90 (approximately Q^2) so Q^3 contributes a much smaller percent in BG compared to TG. This explains why the peak at 493 cm^{-1} is unique in TG spectra.

By comparing Figure 7a and 7c, the transformation from ACP into apatite was significantly decelerated by serum proteins since orthophosphate P-O peaks did not appear until 7 days of immersion in sSBF. The appearance and increasing intensity of the peak at 435 cm^{-1} (Figure 7c) reveals that ACP started to deposit on BG after 2 h immersion in sSBF. This indicates that the crystalline apatite 7 days after immersion in sSBF was derived from ACP. The peaks at 1660 and 1001 cm^{-1} indicate the co-existence of adsorbed proteins with ACP, both of which built up the bio-mineral layer on BG immersed in sSBF (shown in Figure 5a, 5b and 5c). Therefore, the effects of proteins on apatite growth were revealed by combining the results. Serum proteins quickly adsorbed onto the glass surface after immersion in sSBF. Chelation sites on the proteins could have enhanced ACP formation, which together with the adsorbed proteins formed the bio-mineral layers. The interference effects of protein within the bio-mineral layers is likely to have decelerated the transformation of ACP to apatite by inhibiting ion diffusion. This can also explain the smaller dimension of the formed apatite crystals in sSBF (Figure 5c) compared to those formed in pSBF (Figure 2c).

By comparing Figure 7b and 7d, HCA growth was inhibited on TG compared to BG in sSBF, as shown by less in-

Brought to you by | Imperial College London
Authenticated
Download Date | 4/4/19 12:57 PM

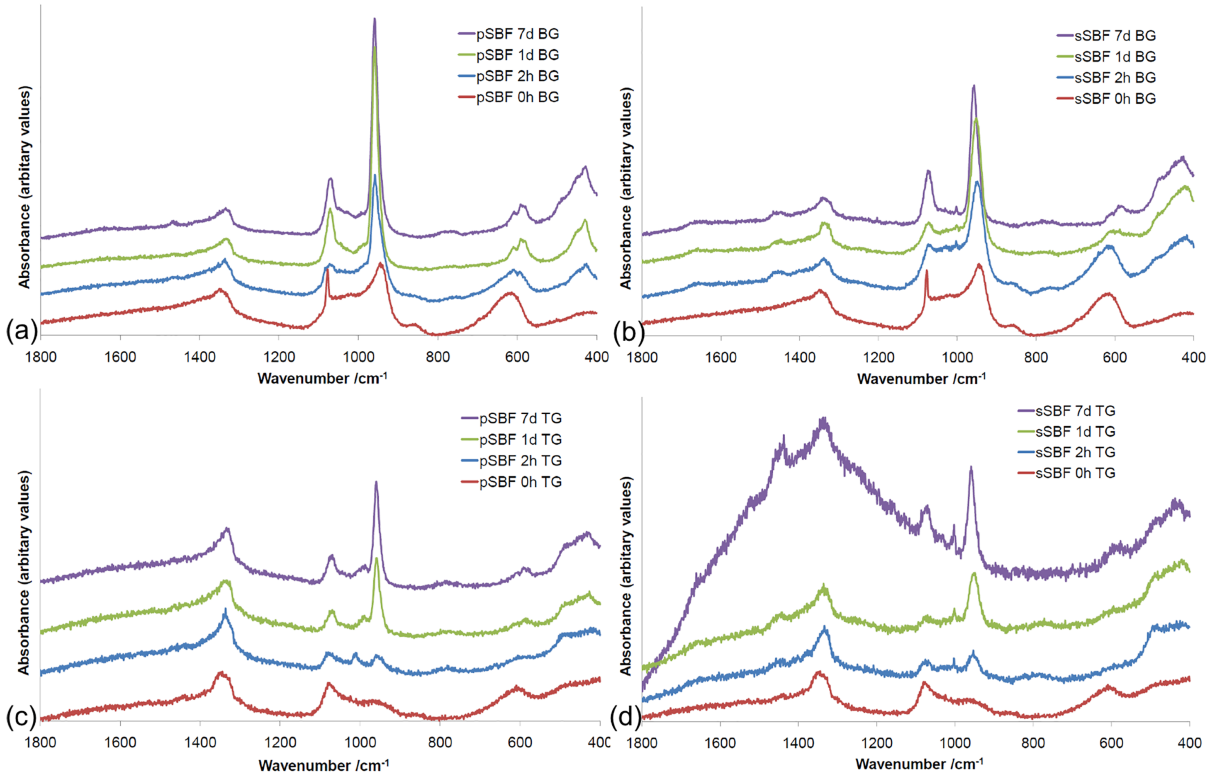


Figure 7: Raman spectra of the glasses as a function of immersion time in media: (a) BG in pSBF; (b) BG in sSBF; (c) TG in pSBF; (d) TG in sSBF.

tensity of the P-O peaks. There are two possible reasons for less phosphate. Firstly, it can be explained by the formation of calcium carbonate, which formed at the expense of phosphate. The higher intensity of peaks at 1660 and 1001 cm^{-1} indicate that TG adsorbed more proteins than BG following immersion in sSBF. The larger amount of adsorbed proteins could cause more inhibitive effects on phosphate formation and is likely to be due to the higher surface area and concave nanoporosity of the TG particles.

To summarise, in the absence of serum protein, HCA growth occurs by calcium phosphate nucleation and HCA crystal growth. This is known to occur through the crystallisation of amorphous calcium phosphate [32]. When serum proteins were present, the amorphous calcium phosphate remained longer, implying that protein adsorption inhibited crystal nucleation and growth. This could be due to a barrier effect, but also due to the adsorbed proteins providing more nucleation sites, which enhance amorphous calcium phosphate growth but also allowing calcium carbonate growth.

3 Conclusions

By comparing the apatite growth on BG and TG in the SBF with and without serum proteins, serum proteins were found to significantly inhibit apatite growth. Apatite growth was enhanced on BG compared to TG due to the lower network connectivity of BG, even though TG has a higher calcium content and high specific surface area. Rapid release of calcium ions does not necessarily lead to more HCA formation. The amorphous calcium phosphate stage in HCA formation is prolonged when serum proteins are present. Calcium carbonate also formed on the sol-gel glass in SBF containing serum, but did not form on the glass in conventional SBF. Calcium carbonate did not form on the 45S5 Bioglass in either condition.

Acknowledgement: EPSRC is thanked for funding via project EP/E057098/1. S. Lin thanks the Society of the Chemical Industry (SCI) for a Messel scholarship (2007-2008) and NovaThera Ltd. (Babraham, UK, no longer operating) for partial funding. Raw data available from rdm-enquiries@imperial.ac.uk.

Brought to you by | Imperial College London
Authenticated
Download Date | 4/4/19 12:57 PM

Conflict of interest: The authors state no conflict of interest.

Ethical approval: The conducted research is not related to either human or animals use.

References

[1] Hench, L.L., Splinter, R.J., Allen, W.C. and Greenlee, T.K., Bonding mechanisms at the interface of ceramic prosthetic materials, J Biomed Mater Res Symp, 1971, 2, 117-141

[2] Hench, L.L., Opening paper 2015- Some comments on Bioglass: Four Eras of Discovery and Development, Biomedical Glasses, 2015, 1, 1-11

[3] Xynos, I.D., Hukkanen, M.V.J., Batten, J.J., Buttery, L.D., Hench, L.L. and Polak, J.M., Bioglass 45S5 stimulates osteoblast turnover and enhances bone formation in vitro: Implications and applications for bone tissue engineering, Calcified tissue international, 2000, 67, 321-329

[4] Jones, J.R., Brauer, D.S., Hupa, L. and Greenspan, D.C., Bioglass and bioactive glasses and their impact on healthcare, Int J Appl Glass Sci, 2016, 7, 423-434

[5] Miguez-Pacheco, V., Hench, L.L. and Boccaccini, A.R., Bioactive glasses beyond bone and teeth: Emerging applications in contact with soft tissues, Acta Biomater, 2015, 13, 1-15

[6] Jones, J.R., Review of bioactive glass: From Hench to hybrids, Acta Biomater, 2013, 9, 4457-4486

[7] Kokubo, T., et al., Ca, P-rich layer formed on high-strength bioactive glass-Ceramic A-W, J. Biomed. Mater. Res., 1990, 24, 331-343

[8] Kokubo, T. and Takadama, H., How useful is SBF in predicting in vivo bone bioactivity?, Biomaterials, 2006, 27, 2907-2915

[9] Macon, A.L.B., et al., A unified in vitro evaluation for apatite-forming ability of bioactive glasses and their variants, J. Mater. Sci. - Mater. Med., 2015, 26, 115-115

[10] Radin, S., Ducheyne, P., Rothman, B. and Conti, A., The effect of in vitro modeling conditions on the surface reactions of bioactive glass, J. Biomed. Mater. Res., 1997, 37, 363-375

[11] Li, R., Clark, A.E. and Hench, L.L., An investigation of bioactive glass powders by sol-gel processing, Journal of Applied Biomaterials, 1991, 2, 231-239

[12] Pereira, M.M., Clark, A.E. and Hench, L.L., Calcium-Phosphate Formation on Sol-Gel-Derived Bioactive Glasses in-Vitro, J. Biomed. Mater. Res., 1994, 28, 693-698

[13] Saravanapavan, P., Jones, J.R., Pryce, R.S. and Hench, L.L., Bioactivity of gel-glass powders in the CaO-SiO2 system: A comparison with ternary (CaO-P2O5-SiO2) and quaternary glasses (SiO_2-CaO-P_2O_5-Na_2O), J. Biomed. Mater. Res. Part A, 2003, 66A, 110-119

[14] Jones, J.R., Ehrenfried, L.M. and Hench, L.L., Optimising bioactive glass scaffolds for bone tissue engineering, Biomaterials, 2006, 27, 964-973

[15] Poologasundarampillai, G., Lee, P.D., Lam, C., Kourkouta, A.M. and Jones, J.R., Compressive Strength of Bioactive Sol-Gel Glass Foam Scaffolds, Int J Appl Glass Sci, 2016, 7, 229-237

[16] Lin, S., Ionescu, C., Pike, K.J., Smith, M.E. and Jones, J.R., Nanostructure evolution and calcium distribution in sol-gel derived bioactive glass, Journal of Materials Chemistry, 2009, 19, 1276-1282

[17] Kokubo, T., Kushitani, H., Sakka, S., Kitsugi, T. and Yamamuro, T., Solution able to reproduce in vivo surface-structure in bioactive glass-ceramic A-W3, J. Biomed. Mater. Res., 1990, 24, 721-734

[18] Hench, L.L., Bioceramics: From Concept to Clinic, Journal of the American Ceramic Society, 1991, 74, 1487-1510

[19] Vallet-Regi, M., Romero, A.M., Ragel, C.V. and LeGeros, R.Z., XRD, SEM-EDS, and FTIR studies of *in vitro* growth of an apatite-like layer on sol-gel glasses, Journal of Biomedical Materials Research, 1999, 44, 416-421

[20] Hill, R.G. and Brauer, D.S., Predicting the bioactivity of glasses using the network connectivity or split network models, J. Non-Cryst. Solids, 2011, 357, 3884-3887

[21] Nommeots-Nomm, A., et al., Highly degradable porous melt-derived bioactive glass foam scaffolds for bone regeneration, Acta Biomater, 2017, 57, 449-461

[22] Lin, S., Van den Bergh, W., Baker, S. and Jones, J.R., Protein interactions with nanoporous sol-gel derived bioactive glasses, Acta Biomater, 2011, 7, 3606-3615

[23] Sepulveda, P., Jones, J.R. and Hench, L.L., Characterization of melt-derived 45S5 and sol-gel-derived 58S bioactive glasses, J. Biomed. Mater. Res., 2001, 58, 734-740

[24] Sepulveda, P., Jones, J.R. and Hench, L.L., In vitro dissolution of melt-derived 45S5 and sol-gel derived 58S bioactive glasses, J. Biomed. Mater. Res., 2002, 61, 301-311

[25] Jones, J.R., Sepulveda, P. and Hench, L.L., Dose-dependent behavior of bioactive glass dissolution, J. Biomed. Mater. Res., 2001, 58, 720-726

[26] Midha, S., van den Bergh, W., Kim, T.B., Lee, P.D., Jones, J.R. and Mitchell, C.A., Bioactive Glass Foam Scaffolds are Remodelled by Osteoclasts and Support the Formation of Mineralized Matrix and Vascular Networks In Vitro, Adv. Healthc. Mater., 2013, 2, 490-499

[27] Porter, A.E., Botelho, C.M., Lopes, M.A., Santos, J.D., Best, S.M. and Bonfield, W., Ultrastructural comparison of dissolution and apatite precipitation on hydroxyapatite and silicon-substituted hydroxyapatite <I>in vitro</I> and <I>in vivo</I>, Journal of Biomedical Materials Research Part A, 2004, 69A, 670-679

[28] Midha, S., Kim, T.B., van den Bergh, W., Lee, P.D., Jones, J.R. and Mitchell, C.A., Preconditioned 70S30C bioactive glass foams promote osteogenesis in vivo, Acta Biomater, 2013, 9, 9169-9182

[29] Sauer, G.R., Zunic, W.B., Durig, J.R. and Wuthier, R.E., Fourier transform raman spectroscopy of synthetic and biological calcium phosphates, Calcified Tissue International, 1994, 54, 414-420

[30] Notingher, I., et al., Application of FTIR and Raman spectroscopy to characterisation of bioactive materials and living cells, Spectroscopy-an International Journal, 2003, 17, 275-288

[31] Yuan, P., He, H.P., Wu, D.Q., Wang, D.Q. and Chen, L.J., Characterization of diatomaceous silica by Raman spectroscopy, Spectrochimica Acta Part A: Molecular and Biomolecular Spectroscopy, 2004, 60, 2941-2945

[32] FitzGerald, V., et al., In situ high-energy X-ray diffraction study of a bioactive calcium silicate foam immersed in simulated body fluid, Journal of Synchrotron Radiation, 2007, 14, 492-499

Brought to you by | Imperial College London
Authenticated
Download Date | 4/4/19 12:57 PM